JOURNAL OF MATERIALS SCIENCE 32 (1997) 2647–2654

Microstructure and mechanical properties of low-pressure injection-moulded reaction-bonded alumina ceramics

M. SAJKO, T. KOSMAČ
Ceramics Department, Jožef Stefan Institute, University of Ljubljana, 1000 Ljubljana, Slovenia

R. DIRSCHERL, R. JANSSEN
Advanced Ceramics Group, Technische Universität Hamburg-Harburg, 21071 Hamburg, Germany

Reaction-bonded alumina was fabricated using standard powder preparation methods and the low-pressure injection moulding (LPIM) forming technique, followed by reaction sintering. The feasibility of LPIM was investigated in terms of the compounding ability of a highly agglomerated mechanically alloyed powder in a non-polar organic vehicle, and the microstructural homogeneity and resulting reliability of sintered LPIM parts. The green density of LPIM parts after debinding, roughly corresponding to the solids loading in the LPIM feedstock, was in the range of fractional density achieved by dry pressing, although the powder packing and aluminium particle deformation during forming were not the same. LPIM forming and debinding induced microstructural inhomogeneities (i.e. larger voids due to trapped air and density fluctuations) which were reflected in a slightly lower Weibull modulus, while the average strength did not differ significantly from the values obtained with dry pressed samples. The microstructure and mechanical properties of sintered parts were also related to the purity of the starting powders. The presence of impurities in the starting aluminium powder resulted in a somewhat coarser microstructure, characterized by a broader Al_2O_3 grain-size distribution, as well as in the presence of a thin glassy phase on the grain boundaries and in partial destabilization of dispersed tetragonal (Y_2O_3-stabilized) ZrO_2 particles. In spite of a less favourable microstructure, the room-temperature strength and Weibull modulus were still comparable to those obtained from high-purity starting powder.

1. Introduction

Reviews of reaction-bonded ceramics, including their generally recognized advantages and drawbacks, were given by Washburn and Coblenz [1] and Chiang *et al.* [2]. Reaction-bonded ceramics (RBC) are fabricated from metallic powder compacts, which are converted to ceramics by reaction with a gaseous phase prior to, or during sintering. This process has been most intensively studied in non-oxide systems, such as reaction-bonded silicon nitride (RBSN) [3] and carbide (RBSC) [4], and is now also successfully applied in oxide systems, such as reaction-bonded alumina (RBAO) [5] and mullite (RBM) [6]. Moderate raw-material costs (depending on purity), low production temperatures and, particularly, low- to zero-shrinkage capability, arising from the volume expansion associated with the metal to ceramic conversion, are the major advantages of RBC. Furthermore, if such a low-shrinkage material can be preformed by a suitable near-net-shaping technique, substantial savings on final machining can be envisaged, resulting in reduced production costs. However, RBC in most cases cannot be fully densified unless additional hot isostatic pressing (HIP) is applied, restricting their use for high performance applications.

The principles of RBAO production, processing techniques and properties have been described in detail by Wu *et al.* [7] and Holz *et al.* [8]. The starting powder mixture containing metallic aluminium (typically 30–60 vol %) and Al_2O_3 is intensively wet-milled to submicrometre-sized particles, dried and compacted. During subsequent heat treatment in air, the metal–ceramic powder compacts are first oxidized and then sintered to final densities. Owing to the fine particle size, most of the metallic aluminium is oxidized at temperatures below the melting point of aluminium. The volume expansion associated with the $Al \rightarrow \alpha\text{-}Al_2O_3$ transition ($\Delta V/V = 28\%$) partially compensates for the sintering shrinkage. Furthermore, the presence of ductile aluminium in the starting

0022–2461

powder mixture provides excellent cold isostatic pressing (CIP) ability, resulting in a rather high (> 65% TD) green density, even without any additional organic binder or plasticizer, and offers sufficiently high strength values for green machining due to some metal–metal contacts in the CIPed green compacts. The "new" Al_2O_3 formed by the oxidation of aluminium acts as a bonding phase between "old" oxide grains. Owing to its clean, glassy phase-free grain boundaries (an important feature of RBAO ceramics), the mechanical strength versus density relation of the sintered material is remarkable, making RBAO ceramics attractive for high-performance structural applications. Furthermore, the mechanical properties of RBAO can be additionally improved by the incorporation of tetragonal ZrO_2 particles, hindering the grain growth of alumina on sintering and crack propagation on loading [9, 10], as in the case of conventional zirconia-toughened alumina (ZTA) ceramics.

For most applications, the choice of materials and selection of processing technique mainly depend on the production costs. RBAO-based ceramics, for example, can be fabricated at lower costs by using cheaper starting powders in combination with low-cost shaping techniques to form green parts. For example, high green densities can be achieved by uniaxial preforming of RBAO powder, followed by CIP. However, only bodies of limited shape can be produced by dry pressing. If, in addition, green machining has to be used to obtain the desired green body geometry, the entire shaping cost can easily exceed acceptable figures, whereas a wet-forming technique providing near-net-shaping might be less cost effective.

Especially in the manufacturing of smaller series of complex-shaped and/or customer-designed ceramic parts, wet near-net shaping methods proved to be competitive to conventional dry pressing methods. Powder injection moulding (PIM) is recognized as one of the most promising techniques which seems to be especially attractive in forming reaction-bonded ceramics, thus combining near-net-shaping and low- to zero-shrinkage material. In PIM the ceramic powder is mixed with molten polymer at temperatures just above the melting point of the organic vehicle. During or after mixing the suspension is degassed and moulded in a cold metallic die, where it solidifies. The moulded parts are then embedded in a high specific surface area powder and subjected to a heat treatment, where the organic binder is removed from the body by capillary wicking, although a small amount of the binder may remain to provide handling strength. Finally, the green bodies are sintered in the desired way [11–13]. During the past 10–15 years in the USA and Japan, rapid technological and commercial progress in high-pressure PIM (HPIM) has been made, so that HPIM using polymer carriers and high injection pressure is now a well-established process for forming high-precision/high-performance heat engine, military, medical, aerospace and automotive parts [12]. The high degree of solids loading and the high moulding pressure results in severe wear of HPIM machine parts and tools, contributing to higher manufacturing costs and restricting the competitiveness of HPIM to a lower series of smaller but complex-shaped parts for high performance. As compared to HPIM, where moulding pressures range from 10–100 MPa and moulding temperatures from 200–300 °C, the low-pressure injection-moulding (LPIM) technique, using a paraffin wax binder system, requires only 0.2–0.6 MPa working pressures and lower temperatures (60–90 °C). Its considerably lower capital investment and lower wear rates of machine parts and moulding tools make LPIM far less expensive than HPIM, at the expense of somewhat lower solids loading in the feedstock, leading to larger shrinkage on sintering, and lower precision of the moulded parts. Because the fractional density of moulded parts after binder removal roughly corresponds to the volume fraction of the solids loading (linear shrinkage on debinding is typically around 1%), it is obvious that a high solids content in the feedstock is one of the most important requirements for LPIM.

In the present work, we report the properties of an RBAO-based material (K20, i.e. RBAO with 20 vol % ZrO_2) produced from inexpensive, less-pure starting powders and formed by LPIM. The feasibility of LPIM was investigated in terms of the compounding ability of a highly agglomerated mechanically alloyed (MA) powder in a non-polar organic vehicle, microstructural homogeneity and the resulting reliability of the sintered LPIM parts. The relationship of the microstructure and mechanical properties of the sintered parts to the purity of the starting powders was also investigated.

2. Experimental procedure

2.1. Materials and processes

The starting powder characteristics and batch compositions are listed in Table I. All starting powder mixtures were wet milled for 7 h at 700 r.p.m. in a 750 cm^3 attrition mill (Netzsch, model PE075) using tetragonal zirconia polycrystalline–TZP (3 mm diameter) grinding bits. As protective liquid, an *n*-hexane solution of Menhaden fish oil (MFO sample A/H) or pure cyclohexane (samples A/C and B/C) was used. Samples from series A were prepared in laboratories at the Jožef Stefan Institute in Ljubljana, whereas samples B were prepared at the Technische Universität Hamburg-Harburg. Before further use, the milled powders were dried, screened and stored in a desiccator. The suspensions for LPIM were prepared by admixing the starting powder mixture into a molten paraffin-wax system (Table II) and subsequent homogenization in a heated three-roller grinding mill (EXACT 80S). Before moulding in a metallic die, suspensions were degassed in a vacuum chamber to remove entrapped air. Rectangular bars ($5 \times 5 \times 45$ mm^3) were moulded at 80 °C using a laboratory LPIM machine of in-house construction. After demoulding, specimens were embedded in a high specific surface area alumina powder (Martinswerk, GX) and slowly heated up to 250 °C for 1 day in order to remove the binder. For comparison, bending strength

TABLE I RBAO powder compositions and main impurity levels

Starting powders		d[a]	Main impurities (wt %)			Composition	
		(μm)	Na_2O	Fe_2O_3	SiO_2	(vol %)	(wt %)
Composition A/H and A/C							
Al	(Exoterm, Kranj)	35	–	0.11 Fe	0.15 Si	45	32
Al_2O_3	(Alcoa A15)	5	0.07	0.01	0.02	35	36
ZrO_2	(Dynazircon F5Y)	0.35	0.03	0.05	0.01	20	32
Composition B/C							
Al	(Alcan 105)	5–50	Trace	0.14 Fe	0.04 Si	45	32
Al_2O_3	(Ceralox MPA-4)	0.5	< 0.01	< 0.005 Fe	< 0.01 Si	35	36
ZrO_2	(Tosoh Co., TZ-2Y)	0.024[b]	< 0.018	0.004	< 0.002	20	32

[a]Average particle size.
[b]Crystallite size.

TABLE II LPIM feedstock formulations for low-pressure injection moulding

Formulation	A/H		A/C	
	(wt %)	(vol %)	(wt %)	(vol %)
RBAO powder	84.1	55.5	86.4	60.0
Paraffin wax[a]	10.2	28.5	9.4	27.6
Synthetic wax[b]	2.2	6.2	2.1	6.2
Octadecylamine[c]	2.2	6.2	2.1	6.2
Menhaden fish oil[d]	1.3	3.6	–	–

[a]Paraffin-wax KX1313, Zschimmer and Schwartz, melting temperature 52–53 °C.
[b]Wax OP, Hoechst, melting temperature 98–102 °C.
[c]Octadecylamine, Aldrich, 90%, melting temperature 52 °C.
[d]Added before milling.

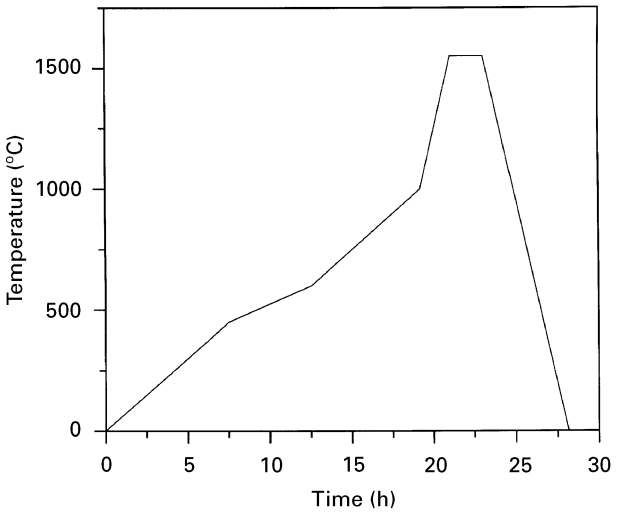

Figure 1 Heating regime for oxidation and sintering of RBAO ceramics.

test bars ($5 \times 4 \times 42\ mm^3$) were compacted by uniaxial pressing at 50 MPa with subsequent cold isostatic pressing at 450 MPa. Both sets of samples, i.e. CIPed and dewaxed LPIM green bodies, were oxidized and sintered at 1550 °C for 2 h in air. The one-step reaction sintering programme is illustrated in Fig. 1.

2.2. Characterization

After milling, powders were characterized by specific surface-area measurements (BET, Perkin–Elmer), determination of the mean particle size and particle-size distribution (laser analyser, Cilas Alcatel) and TGA (Stanton). The green density of dry-pressed parts was calculated from their dimensions and weight, whereas for moulded parts it was estimated from the volume percentage of solids loading in the suspension. Final densities were determined by immersing samples into water and using the Archimedes' principle. Oxidation behaviour was followed by TGA and by monitoring dimensional changes during reaction sintering in a dilatometer (Bähr, Type 802S). Ground and polished test bars, with minimal 13 pieces in each series, were used for four-point bending tests using 10/20 mm measuring spans and $1\ mm\ s^{-1}$ crosshead velocity (Instron, model 1362). Weibull modulus was calculated according to German Standard DIN 51110. For microstructural analysis, specimens were polished and thermally etched (1450 °C, 2 h) in air. On polished and fractured surfaces, microstructure and fracture mode were studied. Average Al_2O_3 and ZrO_2 grain sizes were determined by the linear intercept method. The relative amount of monoclinic and tetragonal ZrO_2 in volume per cent of total ZrO_2 was calculated from the integral intensities of the tetragonal (1 1 1), monoclinic (1 1 1) and (1 1 $\bar{1}$) peaks obtained by XRD of as-sintered and ground surfaces, according to the method of Porter and Heuer [14].

TABLE III Powder characteristics after attrition milling

RBAO powder mixture	d_{50}[a]	BET	Mass gain on oxidation	Al_{remain}[b]
	(μm)	($m^2\ g^{-1}$)	(wt %)	(wt %)
A/H	1.48	10.8	16.0	18.0
A/C	1.70	8.4	15.6	17.5
B/C	1.96	13.0	17.5	19.7

[a]Medium particle size.
[b]Weight per cent of metallic aluminium in the milled RBAO powder as calculated from the mass gain on oxidation.

3. Results and discussion

The RBAO powder characteristics after wet attrition milling are summarized in Table III. Of special interest is the high specific surface area ($>10\ m^2\ g^{-1}$) when compared to the mean particle size (1.5–2 μm),

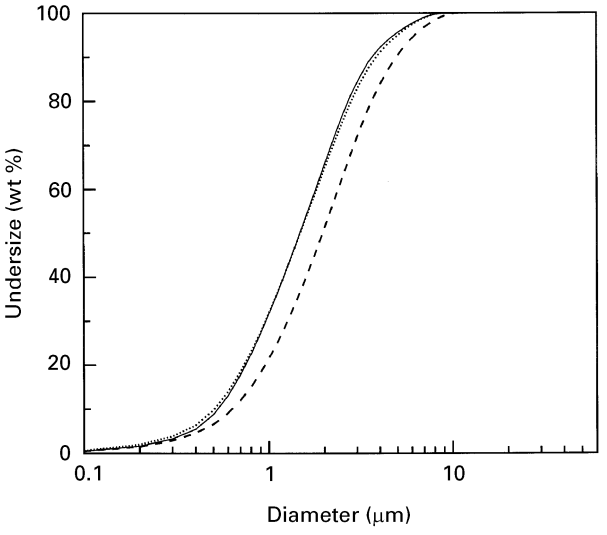

Figure 2 Particle size distribution of various milled RBAO powders. (——) A/C, (- - -) A/H, (– – –) B/C.

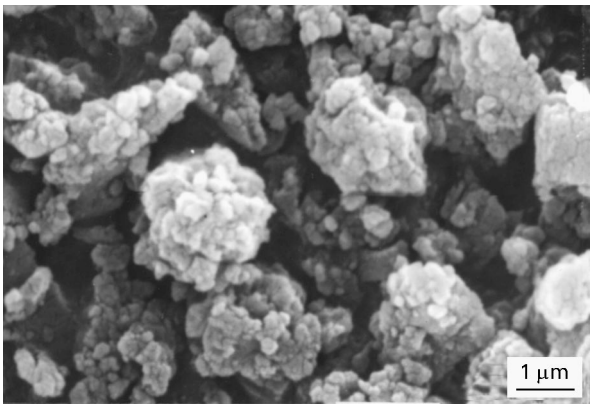

Figure 3 Scanning electron micrograph of RBAO powder A/C after attrition milling in cyclohexane for 7 h at 700 r.p.m.

indicating a high degree of agglomeration and shape complexity of the milled metal–oxide powder mixture. Irrespective of the starting raw materials and protective liquid used, the particle-size distribution after attrition milling is rather broad but still log normal, as shown in Fig. 2. Powders A/H and A/C, which were milled at IJS, differ in average particle size and specific surface area, indicating that the addition of Menhaden fish oil to hexane acts as a dispersant, as in the case of conventional tape-casting formulations. Powder B/C was milled at the Technische Universität Hamburg-Harburg (TUHH) in a larger attrition mill and is therefore somewhat coarser, but the shape of the particle-size distribution curve is nearly the same. The morphology of the RBAO powder A/C after attrition milling is represented in Fig. 3, illustrating the shape complexity, resembling mechanically alloyed (MA) powders.

As is generally known, mechanical alloying (MA) involves repeated plastic deformation, welding and fracturing of metallic particles during highly energetic dry milling. In the early stage of MA, plastic deformation and welding are the predominant processes [15]. With increasing degree of plastic deformation the metallic particles become more brittle, and comminuition, i.e. fragmentation, starts to prevail over welding and agglomeration. During wet attrition milling of an RBAO powder mixture, however, the milling efficiency is much lower (due to the presence of protective liquid), so that work hardening does not lead to an overall embrittlement of the aluminium particles. However, the presence of hard oxide (alumina and zirconia) particles which are indented into plastically deformed aluminium flakes, assists the fragmentation, so that both mechanisms, i.e. agglomeration and comminuition, are taking place, albeit the ductility of metallic aluminium is still preserved. Freshly formed aluminium surfaces react with oxygen and/or water dissolved in the protective liquid, forming oxide or hydroxide layers which, in turn, prevent extensive welding. On the other hand, hydrogen bonding between hydroxyl ($-OH^-$) groups can also lead to the formation of larger agglomerates [16]. Hence, the relatively large mean particle size of milled RBAO powders mainly results from the agglomeration of the fine particles due to metallic and hydrogen bonding.

Before milling, all starting powder mixtures contained 32 wt % of metallic aluminium, which on oxidation should result in a mass gain of 28 wt %. After attrition milling, the observed mass gain deviated from the theoretical value and ranged from 15.6–17.5 wt %, corresponding to 17.5 to 19.7 wt % of metallic aluminium still available for reaction sintering, the balance being oxidized and/or hydrated during milling. In order to estimate the amount of hydrated alumina in the milled powder mixture, TGA was performed in a purified inert atmosphere (N_2, $p(O_2) = 2 \times 10^{-1}$ Pa) which, however, failed to reveal any mass loss due to hydroxide(s) decomposition. The effect was overcompensated by a small but measurable mass gain due to aluminium oxidation resulting from traces of oxygen still present in the system. It was therefore concluded that during wet attrition milling under *n*-hexane or cyclohexane protective liquid, metallic aluminium was in part oxidized rather than hydrated. However, it is worth mentioning that milling in the presence of a larger amount of water in the protective liquid leads to more extensive hydration, which in turn results in a dramatic increase in the specific surface area. Thus, milling in acetone containing larger amounts of water resulted in complete hydration of metallic aluminium, which was accompanied by an increase in the specific surface area from 15 $m^2 g^{-1}$ to 170 $m^2 g^{-1}$. A similar increase in the specific surface area has been observed with AlN powder when reacted with water to form amorphous AlOOH [17] during the initial stage of hydrolysis. It is therefore very likely that hydrated alumina, although undetectable by TGA, also contributes to the increased specific surface area of milled RBAO powder.

Milled powders A/H and A/C differ not only in their average particle size and specific-surface area, but also in the compounding ability and rheological properties of the LPIM feedstock. As briefly mentioned in the experimental section (see also Table II) a mixture of paraffin wax and synthetic wax was

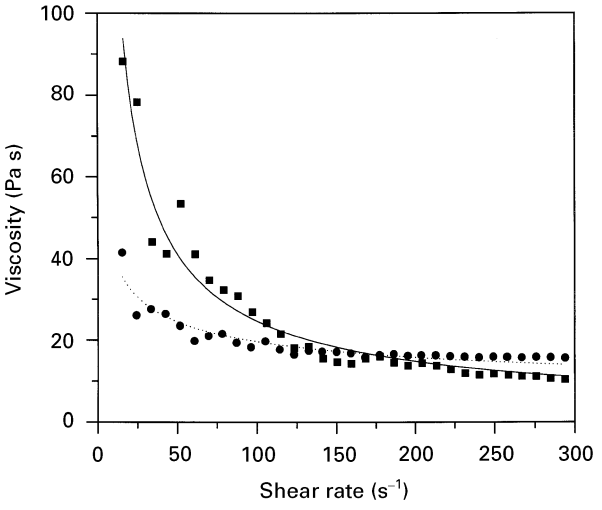

Figure 4 Flow curves of LPIM feedstocks containing RBAO powder milled in various protective liquids: (■) A/H (56 vol % solids loading); (●) A/C (60 vol % solids loading).

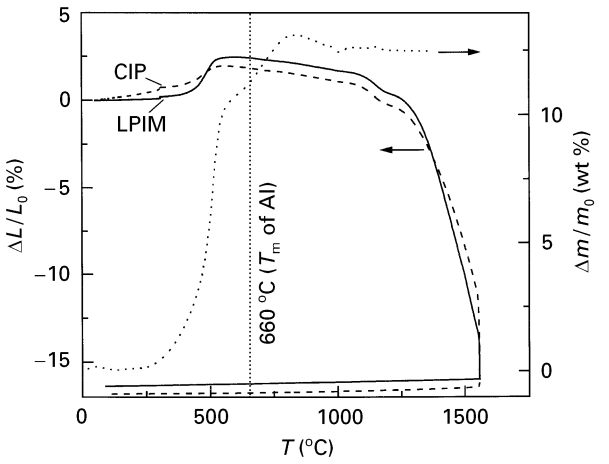

Figure 5 Dilatometric curves of dry pressed (– – –, CIP) and injection-moulded (——, LPIM) powder A/C. (· · ·) The TGA of loose powder A/C. ($\Delta L/L_0$ and $\Delta m/m_0$ are relative length and mass change; T_m is the melting temperature of aluminium).

chosen as the main binder constituent for feedstock preparation. A number of surface-active agents were tested in order to improve the compatibility between RBAO powder and binder. Among them octadecylamine (ODA) proved to be most effective: the addition of 2.2 wt % ODA with respect to the solids enabled the attainment of more than 60 vol % solids loading in the feedstock at an acceptable viscosity for LPIM (viscosity $\eta < 30$ Pas at a shear rate $D > 10\,s^{-1}$). The flow behaviour of A/C and A/H feedstock with the compositions listed in Table II are represented in Fig. 4. The presence of Menhaden fish oil, which proved to be beneficial during wet attrition milling, diminishes the effectiveness of ODA in improving the compounding ability of powder A/H by reducing the maximum attainable solids loading (56 vol % versus 60 vol % for powder A/C) and by increasing the pseudoplasticity of the feedstock, as shown in Fig. 4. In PIM practice, pseudoplasticity of the feedstock (i.e. a noticeable drop in viscosity with increasing shear rate, which is a commonly observed feature in concentrated ceramic suspensions) is usually thought to be beneficial, because it prevents deformation of moulded parts during the debinding operation [12, 18]. However, our injection-moulding experiments showed that pronounced pseudoplasticity of the feedstock A/H exerts a negative influence on the de-airing and moulding ability by increasing the number and size of macroscopic voids in LPIM parts.

The compounding ability of milled RBAO powder was even more detrimentally influenced by the addition of a small amount (1–2 %) of water to the protective liquid. As already mentioned, water promotes hydration of metallic aluminium, thereby increasing the specific surface area of the powder mixture ($\sim 23\,m^2\,g^{-1}$). In addition, it has the ability to be preferentially adsorbed on to the particle's surface, causing flocculation and decreasing the wettability of solid particles by the paraffin-based organic vehicle. As a consequence, no more than 48 vol % solids loading could be attained in such a feedstock which, in addition, exhibited highly unfavourable rheological properties, i.e. high pseudoplasticity and thixotropy.

Dilatometric curves of the material A/C (Fig. 5) show a noticeable difference in the oxidation and sintering behaviour of samples formed by LPIM and dry-pressing. In the former case the oxidation seems to occur at higher temperatures, and the extent of expansion associated with oxidation is considerably larger than in the case of the dry-pressed sample. Although both green pellets had approximately the same fractional density (60 % theoretical density), they differed in their pore-size distribution and interparticle bonding. During dry pressing, metallic aluminium is additionally plastically deformed, resulting in an increased interparticle contact area and bonding strength. In contrast, during wet forming by LPIM no plastic deformation occurs. On the other hand, thermal debinding is accompanied by particle rearrangement and migration of finer particles toward the surface, thereby altering the structure of the interconnected porosity and, to a certain extent, creating density gradients from the surface toward the interior of the moulded specimens. After debinding, the green parts still contain several per cent (3–5 wt %) of binder (to provide sufficient green strength for handling) and the remaining organic thin film is believed to protect the metallic aluminium against oxidation, which cannot start unless the binder is completely removed. It is also assumed that weak interparticle bonding after binder removal allows considerably larger expansion of the green parts on oxidation, as compared to dry-pressed green bodies.

Fig. 5 also shows the TG behaviour of dried powder A/C after milling, which was monitored under the same heating conditions as the sintering experiments (see also Fig. 1). According to TGA, most of the metallic aluminium is oxidized by the solid–gas reaction below the melting point of aluminium (660 °C). Initially, the oxidation rate is very high, but at about 550 °C it slows down and increases again above the melting point of aluminium, until at about 900 °C oxidation is complete. Similar TG behaviour was also

reported by Wu *et al.* [7], who distinguished two temperature regions of oxidation below the melting point of aluminium. It is suggested that the oxidation of metallic aluminium is controlled by the formation of microcracks in the oxidized layer, through which oxygen can reach the metallic surface. In the temperature region from 450–540 °C, most of the subcritical sized particles are oxidized violently, while the reaction slows down between 540 and 660 °C, where oxide skin cracking of supercritical-sized particles cannot take place until a metallic melt is formed, which is accompanied by an additional volume expansion of 11%. From the results of thermal analysis represented in Fig. 5, it can thus be concluded that only the initial stage of oxidation is accompanied by the volume expansion of green RBAO parts. During the next two oxidation stages the material starts to shrink steadily, presumably due to the crystallization and densification of freshly formed transient alumina, until at about 1100 °C intensive sintering occurs. The discontinuity in the sintering behaviour between 1150 and 1200 °C coincides with the $\gamma \rightarrow \alpha Al_2O_3$ transition, but may also result from differential sintering due to the presence of agglomerates.

The microstructural characteristics of sintered RBAO specimens are presented in Table IV, together with the average bending strength values and corresponding σ_0 and m values, obtained by Weibull's statistical analysis. The sets of sintered specimens differ in the purity of the starting powders (powder mixtures A versus B), the protective liquid used for attrition milling (*n*-hexane containing MFO versus cyclohexane) and green body forming technique (LPIM versus dry pressing). As already mentioned, the compounding ability of powder A/H to form LPIM feedstock was not as good as that of powder A/C, reflected in poor moulding ability. In spite of this, some of the moulded samples were sintered and subjected to bending tests. Although the number of tested specimens is not sufficient for a rigorous assertion, the mean value (average of five measurements) is included in Table IV, together with the standard deviation. The sintered density of all LPIM specimens was noticeably influenced by the presence of larger spherical voids originating in the air trapped in the feedstock and, to a certain extent, in the existence of a less-dense central region (porous core) in the sintered parts. A porous core is a commonly observed defect in sintered parts formed by LPIM, especially if the wall thickness is large and the solids content in the feedstock is low. In spite of numerous macroscopic defects present in the samples, the lowest bending strength value was as high as 386 MPa, confirming the potential of RBAO ceramics for structural applications. The better compounding ability of powder A/C resulted in a high solids loading in the corresponding LPIM feedstock, and consequently in higher green and sintered densities. The somewhat lower sintered density of the LPIM A/C material as compared to dry-pressed A/C is mainly due to the presence of some larger spherical voids arising from trapped air in the moulded parts, whereas a porous core was not observed in these samples. To a certain extent, the source of larger voids can be diagnosed by analysing the pore geometry (spherical or elongated) and position (central, top, random); their elimination, however, is not easy but is feasible. It is worth mentioning that the dry-pressing ability of powder A/C without any binder addition was not as good as reported in the literature. Namely, density gradients and lamination were quite commonly observed defects in dry-pressed A/C samples. It is therefore not surprising that the mean bending strength and Weibull modulus of the LPIM and dry-pressed A/C samples were nearly the same. Taking into account the relatively high residual porosity and the presence of larger defects arising from forming green parts, the strength and reliability of RBAO ceramics are remarkable, regardless of the green body forming technique used. Furthermore, because the bending strength and corresponding Weibull modulus of sintered B/C material are not superior to those of the A/C material, the performance of RBAO ceramics (at least at room temperature) does not seem to be extremely sensitive to the purity of the starting powder either. Scanning electron micrographs of sintered A/C and B/C samples (Fig. 6a and b) revealed, however, that the purity of starting powders plays an important role in grain growth during sintering. The microstructure of sintered A/C material is considerably coarser than that of B/C material, e.g. the mean alumina grain size of A/C is approximately 1.5 times larger than in B/C. This was tentatively attributed to a higher impurity level in the starting powder mixture A, especially to a higher silicon content in the starting aluminium

TABLE IV Microstructural characteristics and corresponding mechanical properties of RBAO ceramics formed by LPIM and dry-pressing

Sample	Forming technique	ρ_0[a] (%)	ρ_s[a] (%)	d_{ZrO_2}[b] (μm)	$d_{Al_2O_3}$[b] (μm)	$\sigma_{b,4p}$[c] (MPa)	σ_0[d] (MPa)	m[d]
A/H	LPIM	56[a]	93	0.54	1.14	473 ± 76[f]	–	–
A/C	LPIM	60[e]	95	0.45	1.21	473	502	7.8
	Dry pressed	60	97	–	–	467	495	8.1
B/C	Dry pressed	60	96	0.42	0.79	545	–	9

[a] ρ_0, green density; ρ_s, sintered density.
[b] d_{ZrO_2}, $d_{Al_2O_3}$, average size of the grains on a polished sintered surface.
[c] $\sigma_{b,4P}$, average value of four-point bending test measurements.
[d] $\sigma_{0,}$, m, normalized bending strength (at the fracture probability of 63.2%) and Weibull modulus from the Weibull's distribution function: $P(\sigma) = 1 - \exp(-\sigma/\sigma_0)^m$; where P is a fracture probability and σ is applied bending stress.
[e] Calculated from solids loading.
[f] Average value of five measurements.

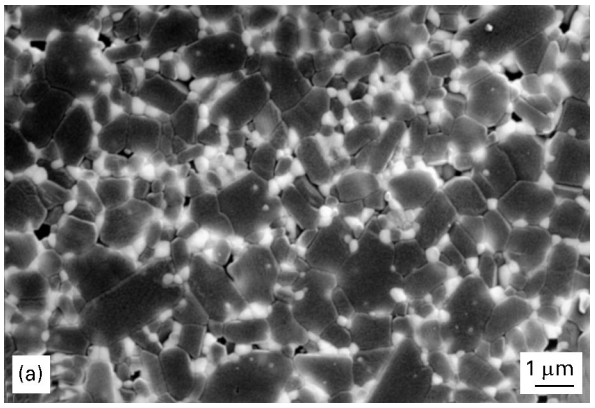

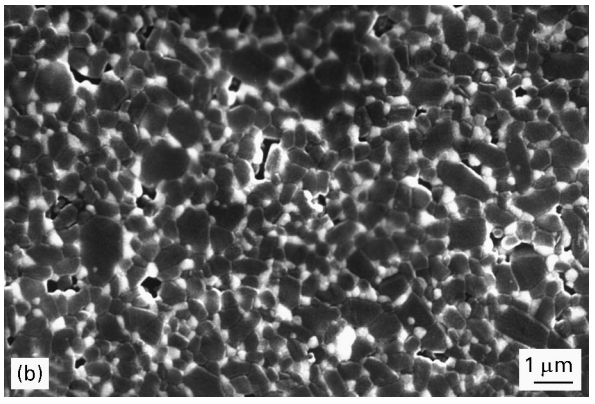

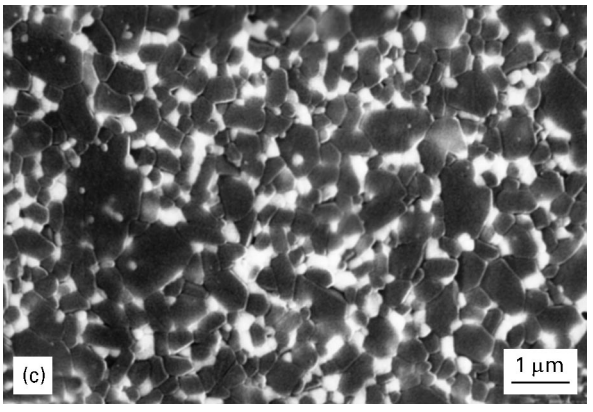

Figure 6 Scanning electron micrographs of sintered (2 h at 1550 °C), polished and thermally etched RBAO samples. (a) A/C, (b) B/C and (c) B/C contaminated by the addition of 0.3 wt % calcined kaolin.

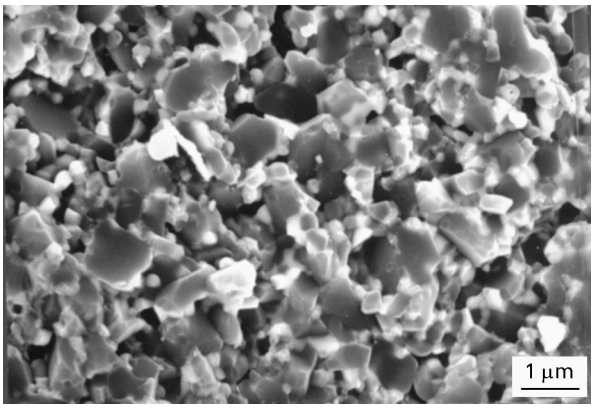

Figure 7 Scanning electron micrograph of fracture surface of RBAO sample A/C after sintering for 2 h at 1550 °C.

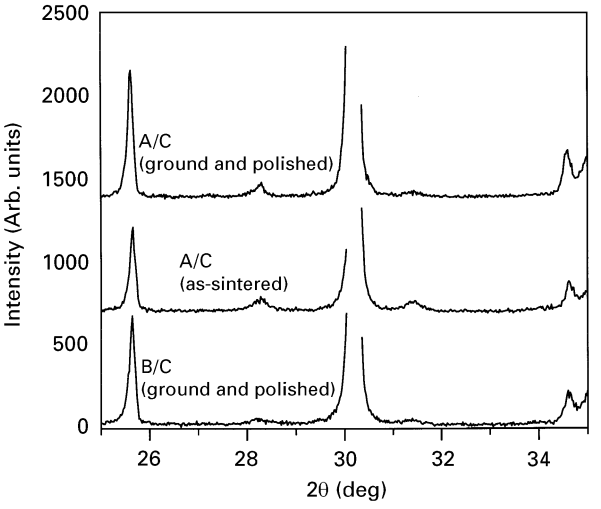

Figure 8 X-ray diffraction pattern of sintered A/C and B/C samples before and after grinding with a 180 μm diamond grit.

powder. Namely, the presence of a small amount of silicate phase was shown to promote alumina grain growth during sintering of conventional ZTA ceramics, which in turn leads to zirconia grain coarsening and a higher amount of intragranular zirconia particles [10] also found in sintered RBAO. To verify this assumption, a small amount of calcined kaolin (0.3 wt %) was admixed to the starting powder mixture B, resulting in alumina grains 1.4 times larger after sintering (Fig. 6c). A high-resolution electron micrographic analysis of A/C revealed the presence of a thin (2 nm) amorphous layer on alumina grain boundaries (to be published elsewhere), giving further support to the assumption that the grain growth in A/C RBAO was promoted by the glassy phase. In spite of the presence of this glassy phase on the grain boundaries, the room-temperature fracture of A/C material remains predominantly transgranular, as illustrated in Fig. 7. The presence of liquid silicate phase during sintering not only promotes grain growth, but according to the literature [19] also has the ability to dissolve Y_2O_3 from YTZP. It is well known that the stability of dispersed tetragonal ZrO_2 particles in a ceramic matrix decreases with decreased Y_2O_3 content and increased ZrO_2 grain size. Destabilization leads to the tetragonal → monoclinic phase transformation of dispersed ZrO_2 particles, which may occur either spontaneously during cooling from the sintering temperature, or can be induced by an externally applied stress. In fact, about 5 vol % total ZrO_2 was spontaneously transformed into the monoclinic form on cooling specimens A/C, and an additional 4 vol % on grinding these specimens, whereas only traces of m-ZrO_2 were observed in sintered and ground specimens B/C (Fig. 8). It is therefore assumed that the high transformability of dispersed zirconia particles also contributes to the relatively high room-temperature strength of RBAO ceramics containing glassy phase grain boundaries.

4. Conclusions

In the present work it was demonstrated that LPIM can be used for forming and manufacturing of RBAO ceramics. Also, high-purity starting powders can be replaced by inexpensive, less-pure raw materials, at the expense of a less-homogeneous microstructure and a minor reduction in room-temperature strength.

The compounding ability of highly agglomerated RBAO powder after attrition milling is sensitive to the protective liquid used during milling, especially to the presence of water. The presence of residues of the organic vehicle and the weak interparticle bonding in LPIM formed green bodies results in retarded onset of oxidation and (higher) larger volume expansion associated with the initial stage of oxidation, as compared to CIPed green bodies. After sintering, however, the microstructural characteristics, mean bending strength and Weibull modulus are almost the same for CIPed and LPIM formed samples. On the other hand, the purity of starting powders proved to play by far a more important role in the microstructure and mechanical properties of sintered RBAO ceramics than the forming technique. A higher impurity level, in particular a higher silicon content, leads to glassy phase formation during sintering, which promotes alumina and zirconia grain growth and also has the ability to dissolve yttria from YTZP grains, thereby increasing the transformability of dispersed zirconia grains. In spite of a somewhat coarser microstructure and a thin glassy phase containing grain boundaries, the fracture of such a material remains predominantly transgranular, resulting in a room-temperature strength and Weibull modulus comparable to those obtained from high-purity starting powders.

Acknowledgement

The work was performed within the bilateral Slovenian–German Cooperation in Scientific Research and Technological Development. The financial support of the Internationales Büro der KFA Jülich and Slovenian Ministry of Science and Technology is gratefully acknowledged.

References

1. M. E. WASHBURN and W. S. COBLENZ, *Ceram. Bull.* **67** (1988) 356.
2. Y. CHIANG, J. S. HAGGERTY, R.P. MESSNER and C. DEMETRY, *ibid.* **68** (1989) 420.
3. J. MOULSEN, *J. Mater. Sci.* **14** (1979) 1917.
4. P. POPPER, Special Ceramics (Heywood, London, 1960) p. 209.
5. N. CLAUSSEN, T. LI and S. WU, *J. Eur. Ceram. Soc.* **5** (1989) 29.
6. S. WU and N. CLAUSSEN, *J. Am. Ceram. Soc.* **74** (1991) 2460.
7. S. WU, D. HOLZ and N. CLAUSSEN, *ibid.* **76** (1993) 970.
8. D. HOLZ, S. WU, S. SCHEPPOKAT and N. CLAUSSEN, *ibid.* **77** (1994) 2509.
9. T. KOSMAČ, M. V. SWAIN and N. CLAUSSEN, *Mater. Sci. Eng.* **71** (1985) 57.
10. T. KOSMAČ and A. KRELL, *PMI* **5** (1993) 229.
11. P. O. GRIBOVSKIJ "Gorjačee litie keramičeskih izdelij" (Gosudarstvennoe energičeskoe izdatelstvo, Moskva-Leningrad, 1961).
12. R. M. GERMAN, "Powder Injection Moulding" (Metal Powder Industries Federation, Princeton, NJ, 1990).
13. J. A. MANGELS, *Am. Ceram. Soc. Bull.* **73** (1994) 37.
14. D. L. PORTER and A. H. HEUER *J. Am. Ceram. Soc.* **62** (1979) 298.
15. T. H. COURTNEY, B. J. M. AIKING, D. MAURICE, R. W. RYDIN and T. KOSMAČ, in "Proceedings of the 2nd International Conference on Structural Applications of Mechanical Alloying", Vancouver, British Columbia, Canada (ASM International, Ohio, 1993) p. 1.
16. S. REED, "Introduction to the Principles of Ceramic Processing" (New York State College of Ceramics, Alfred University, Wiley-Interscience, New York, 1988).
17. P. BOWEN, J. G. HIGHFIELD, A. MOCELLIN and T. A. RING, *J. Am. Ceram. Soc.* **73** (1990) 724.
18. M. J. EDERISINGHE and J. R. G. EVANS, *J. Mater. Sci.* **22** (1987) 269.
19. J. HOLC, *Solid State Ionics* **68** (1994) 331.

Received 5 March
and accepted 30 October 1996